Targeted imaging in oncologic surgery : preclinical studies utilizing near-infrared fluorescence and radioactivity

Boonstra, M.C.

Chapter 8

Preparation of the zwitterionic near-infrared fluorescent peptide cRGD-ZW800-1 for clinical trials in image-guided cancer surgery

Supplementary data on ePUB

ABSTRACT

Purpose: Incomplete resections and damage to critical structures downgrade patient prognosis and increase morbidity. Targeted fluorescence imaging aids surgeons by accurate and real-time detection of tumors and vital structures. This study prepares the tumor-targeted zwitterionic near-infrared fluorescent peptide cRGD-ZW800-1 as an intraoperative imaging agent for clinical use.

Experimental Design: cRGD-ZW800-1 was synthesized via current Good Manufacturing Practices and extensively characterized *in vitro* and *in vivo*, including pharmacokinetics and toxicology.

Results: After synthesis and HPLC purification, cRGD-ZW800-1 was sterilely aliquoted into 10 mL glass vials containing 0.725 mg product and lyophilized. cRGD-ZW800-1 was satisfactorily stable, showed no significant degradation in water or sera and internalized after cell binding. Biodistribution showed high signals in tumors and metabolizing organs. Dose finding studies provided an optimal dose of 10 nmol, corresponding to a human equivalent dose of 63 µg/kg and an optimal imaging window between 4-24 h post-injection. cRGD-ZW800-1 has a serum half-life of approximately 25 min (clearance of 0.25±0.05 mL/min) and provided fast and accurate tumor identification in clinically relevant human xenograft mouse models of colorectal, pancreatic and head-and-neck cancer. Toxicology studies showed a no observable adverse event level (NOAEL) in rats at doses of at least 5.0 mg/kg and an initial dose for human clinical trials could therefore be set at 80 µg/kg.

Conclusions: Due to the recognition of multiple integrins, associated with malignant and neoangiogenic cells, it is expected that cRGD-ZW800-1 will provide a robust, sensitive, and universal tool to detect (residual) cancer during surgery and to improve clinical outcomes considerably.

Statement of clinical relevance

A patient's prognosis after cancer surgery depends mainly on the completeness of surgical resection and the amount of damage to critical surrounding structures. Targeted fluorescent imaging agents are moving towards the clinic and enable accurate identification of tumors and other structures in real-time during surgery. This preparatory study provides the basis for the clinical introduction of the zwitterionic near-infrared (NIR) fluorescent peptide cRGD-ZW800-1. As RGD-recognizing integrins are located throughout many tumors and their microenvironment, this agent can be widely applied and should have broad clinical value. Targeted fluorescence imaging will bring surgery to the next level; visualizing otherwise invisible structures and lesions making surgery safer and more precise. It is expected that cRGD-ZW800-1 will provide a robust, sensitive, and selective tool to detect (residual) cancer during surgery and to improve clinical outcomes.

INTRODUCTION

Accurate and real-time detection of tumors and vital structures during surgery remains challenging. Analogous to single-photon emission computed tomography (SPECT) and positron emission tomography (PET) agents, tumor targeting ligands can also be conjugated to near-infrared (NIR, 700-900 nm) fluorophores, permitting real-time visualization during surgery using dedicated intraoperative imaging systems [1, 2]. Traditionally, NIR fluorophores have been used for a variety of preclinical applications mainly to monitor the fate of intravenously administered anticancer therapeutics like monoclonal antibodies for determining biodistribution, tissue penetration, and cellular localization [3]. Currently, a variety of NIR fluorophore labeled ligands are specifically evaluated as real-time diagnostic tools for accurate localization of cancer cells and vital structures during surgery. These ligands range from (therapeutic) monoclonal antibodies and antibody fragments to larger and smaller peptides mimicking natural receptor ligands, such as GE-137 for c-MET (HGFR), synthetic folate for the folate receptor-α (FR-α) and the arginyl-glycyl-aspartic acid (RGD) binding to various integrins [4, 5].

Introduction of the fluorescence optical imaging technique in humans after administration of synthetic folate conjugated to the fluorophore FITC (500 nm emission) to patients with suspected ovarian cancer showed promising results [6]. However, the clinical value of this probe might be limited due to the selective overexpression of FR-α [7, 8] and the use of the 500 nm wavelength fluorophore that suffers from autofluorescence and the inability to detect deeper located lesions [9]. Being one of the first human studies of

fluorescent ligands, dose-selection and the time frame between administration of the dye and surgery were rather arbitrary for this particular imaging compound.

Here we evaluate cRGD-ZW800-1, a cyclic pentapeptide conjugated to the zwitterionic 800 nm NIR fluorophore ZW800-1 [10]. RGD is clinically well-known and binds to various integrins (αvβ1, αVβ3, αvβ5, αvβ6, αvβ8, α5β1, α8β1 and αIIbβ3) mostly associated with neoangiogenesis. Overexpression of these integrins is found in breast, colorectal, pancreas, brain, and lung cancers if these tumors grow larger than 1-2 mm [11, 12]. RGD-based molecules have been extensively investigated in various phase I and phase II PET and SPECT imaging studies and in a phase III study as an anticancer therapy (cilengitide) [13-20]. Beer et al. investigated biodistribution, pharmacokinetics and tumor uptake of the PET-tracer 18F-galacto-RGD in melanomas, (metastatic) breast cancer, head-and-neck cancer, and in glioblastomas [13-15]. These data suggested rapid blood clearance (optimal tumor-to-background ratio, TBR, after 72 min), uptake in all invasive carcinomas (including lymph node metastasis), a sensitivity of 76% compared with clinical staging, and a high correlation between signal and αVβ3 expression on endothelial and malignant cells. Use of the cRGD-based SPECT tracer 99mTc-NC100692 allowed identification of 9 out of 11 highly suspicious breast tumors as malignant and detection of metastases from lung and breast cancer [17, 18].

RGD has previously been conjugated to IRDye800CW, ZW800-1, and other fluorophores for optical imaging applications. cRGD-IRDye800CW showed delineation of glioblastomas in xenograft mouse models and underscored the relative simplicity and low cost of the synthesis in combination with the rapid clearance character of RGD based NIR fluorescent agents [21]. Extensive preliminary work on the development and evaluation of cRGD-ZW800-1 agent has been performed by our group and showed clear delineation of melanomas and colorectal, liver, and lung tumors in xenograft mouse models [4]. Moreover, due to its predominant renal clearance, ureters could also be recognized, which can prevent damage to these structures during surgery in the lower pelvis [22]. Zwitterionic NIR fluorophores also have the distinct advantage of much lower non-specific uptake in normal tissues and organs compared to conventional anionic NIR fluorophores [4, 10].

This preclinical study was performed to permit administration of cRGD-ZW800-1 in Phase I clinical trials and describes the complete clinical development path, including current Good Manufacturing Practices (cGMP) production, *in vivo* toxicity tests, and measurement of pharmacokinetics (PK) and pharmacodynamics (PD).

MATERIALS AND METHODS

GMP production and purification of cRGD-ZW800-1

General remarks, chemicals, synthetic procedures, and purification are extensively described in the supplementary data.

Stability of cRGD-ZW800-1

A stock solution of 0.5 mg/mL of cRGD-ZW800-1 in PBS was prepared. Half of the stock solution was kept exposed to light and the other half was stored in the dark, both at room temperature. UPLC-MS (Waters BEH C18 130 Å 1.7 µm (100 × 2.1 mm) column) analysis was performed at t = 0, 1, 4, 22, 46, 72, 96 h as described in the supplementary data.

Furthermore, cRGD-ZW800-1 was prepared at 40 µM, 4 µM, and 0.4 µM in rat K2-EDTA plasma. Samples were incubated at +37°C (t=0, 1, 2, 4, 6 and 24 h). Sample cleanup was performed by adding 400 µL CH3CN to 200 µL plasma to crush the proteins. Samples were vortexed, centrifuged (5 min, 5500xg), and the supernatant was subsequently stored on melting ice (0°C) until analysis. Calibrators were prepared in the range: 0.15 – 60 µM. The extract was injected into an UHPLC system (Agilent 1290 series; Hewlett Packard, Palo Alto, CA, USA) equipped with a Sciex API5500 Qtrap mass spectrometer (Applied Biosystems, Foster City, CA, USA). The analytical column used was an Xbridge CX18 100x4.6 mm (3.5 µm) column (Waters, Milford, MA, USA). The following LC solvent program (500 µL/min) was used: 5% CH3CN in Milli-Q water (solvent A), 5% CH3CN in Milli-Q water with 1% FA (solvent B) and CH3CN (solvent C). A linear gradient was set from 0-4.0 min (85% A, 10% B, 5% C); 4.0-5.1 min (40% A, 10%B, 50% C) and finally, 5.1-8 min (85% A, 10% B, 5% C). The tandem mass spectrometry system was operated in positive ion mode using full scans of 250 – 1000 m/z (EMS) and/or 100-1000 m/z (EPI).

Stability of cRGD-ZW800-1 was also measured by VIS-NIR absorbance spectrophotography. cRGD-ZW800-1 was diluted in 0.05 mM HEPES buffered water, mouse, rat, and human serum to a concentration of 5.0 µM. Mouse, rat, and human serum without cRGD-ZW800-1 was included as controls. All samples were incubated at 37°C in the dark. Subsequently, absorbance was measured using the Ultrospec 3000 UV/visible spectrophotometer (Biochrom Ltd., Cambridge, United Kingdom) using full spectrum scans (200 – 1000 nm). Measurements were performed for 1 to 240 minutes.

To evaluate serum binding, cRGD-ZW800-1 was incubated in PBS and human serum for 1 and 4 h before gel electrophoresis (SDS-PAGE gel, 4-20%) was performed. To visualize cRGD-ZW800-1 the gel was scanned using the Odyssey imager (LI-COR Biosciences, Lincoln, Nebraska: 800-nm channel).

Human cancer cell-lines, flow cytometry and binding assays

Colorectal (HT-29-luc2), pancreatic (BXPC-3-luc2), and oral squamous tongue carcinoma (OSC-19-GFP-luc2) cells were previously described [41, 42] and described in the supplementary data. Qifikit (DAKO) was used to determine the number of antigenic sites for the three most commonly described integrins: αVβ3, αvβ5, and αvβ6. These procedures were previously described [43] and detailed in the supplementary data, together with the procedures for the binding assays [41, 43].

Animal models

Six week-old athymic female mice (CD1-Foxn1nu, Charles River Laboratories, Wilmington, MA, USA) were used and housed in ventilated cages. Normal pellet food and sterilized water were provided *ad libitum*. Throughout tumor inoculation and imaging procedures, animals were anesthetized with isoflurane. The Animal Welfare Committee of Leiden University Medical Center approved all animal experiments for animal health, ethics, and research. All animals received humane care and maintenance in compliance with the "Code of Practice Use of Laboratory Animals in Cancer Research" (Inspectie WandV, July 1999).

To induce subcutaneous tumors, HT-29-luc2 cells were injected at 4 sites on the back (500,000 cells per spot). Colonic orthotopic tumors were generated as described by Tseng *et al*. [44], orthotopic pancreatic tumors were induced as previously described by Kim *et al*. [45] and the head-and-neck cancer tumors were induced as previously described by van Driel et al.[42]. All procedures are briefly described in the supplementary data.

After imaging, mice were sacrificed, organs were collected and exposed to evaluate the biodistribution pattern, and tumors were quick frozen in isopentane at -80°C for histological evaluation. Tissues were sectioned at 10 μm and fluorescence imaging was performed using fluorescence microscopy (Nikon eclipse e800, Nikon, Amsterdam, The Netherlands). All histologic sections were stained with standard hematoxylin-eosin stain (HE).

NIR-fluorescence imaging systems

Real-time NIR-fluorescence measurements and fluorescence-guided resections were performed using the FLARE® Prototype NIR imaging system [46]. The Pearl® Impulse small animal imaging system (LI-COR) was used as an *in vivo* preclinical reference system to measure NIR-fluorescence signals for bio-distribution analysis and to calculate TBRs. The specific and control images were normalized and regions of interest (ROIs) were selected using associated software. Using the FLARE® software no semi-quantitative intensity/ pseudo-color scale bars could be generated therefore in each image the TBRs

are mentioned to semi-quantify the fluorescent signals. TBR was calculated by dividing the tumor signal by the background signal. A sufficient TBR was considered to be ≥2.0.

In vivo specificity

The binding specificity of cRGD-ZW800-1 was explored by blocking the integrins using an excess of unlabeled cRGD (200-fold excess) co-injected with a standard dose of 10 nmol cRGD-ZW800-1 (n=4). Simultaneously, mice (n=3) were injected with 10 nmol cRGD-ZW800-1 as positive control. Images were acquired at 4 and 24 h post-injection after which animals were sacrificed and organs were resected and scanned with both the Pearl® and FLARE® Prototype imaging system.

In vivo binding characteristics and biodistribution

Mice were administered with 0.25 (0.39 µg), 1 (1.5 µg), 10 (15.5 µg), or 30 nmol (46.4 µg) cRGD-ZW800-1 to evaluate tumor signals, biodistribution, and to calculate TBRs. At 4 and 24 h after injection, mice were fully dissected and their organs were measured for fluorescence. Signal-to-background ratios were calculated by dividing the mean fluorescence signals of tissues by the mean of the surrounding tissues or blood.

Pharmacokinetics

cRGD-ZW800-1 was diluted in 0.05 mM HEPES buffered mouse serum to the concentrations 5.00, 4.50, 4.00, 3.50, 3.00, 2.50, 2.00, 1.50, 1.00, 0.50, 0.25, 0.13, 0.06, 0.03, and 0.02 µM. A calibration curve was created by measuring each concentration in 60 µL capillary tubes (Hirschmann® Laborgeräte GmbH and co. KG, Eberstadt, Germany) using the FLARE® Prototype with exposure times of: 1, 2, 5, 10, 25, 50, 100, 200, 500, 1000, and 2000 ms. Data were plotted in fluorescence intensity over concentration (µM) (Figure S7). For each exposure time, the formula of the linear regression line was calculated. Subsequently, 5 mice were injected with 10 nmol cRGD-ZW800-1 via the lateral tail vein. The contralateral lateral tail vein was used to draw blood on the time points -5, 1, 6, 10, 20, 30, 40, 50, 60, 90, 120, and 240 min. post injection. Blood samples were absorbed using 60 µL capillary tubes and immediately measured using the FLARE® Prototype with the same exposure times. Saturated images and those under the detection limit were excluded from analysis. Each measurement was calculated back to its concentration using the matching formulas. The mean of each formula output was used as the concentration. Data was analyzed using NONMEM® software (Icon Development Solutions, Ellicott City, MD, USA). Data were plotted in logarithmic and linear concentration (µM) over time (min).

Toxicology test system

A generic extended single dose intravenous non-clinical toxicity study was performed according to ICH M2 (R2), FDA, EMEA and GLP regulations. Methods are described in the supplementary data.

Statistical analysis

For statistical analysis and the generation of graphs, GraphPad Prism software (version 5.01, GraphPad Software Inc., La Jolla, California, USA) was used. Differences between groups in the immunofluorescence assays were analyzed using the Mann-Whitney U test. Relations between TBRs were calculated using the two-way repeated measurement ANOVA (corrected using Bonferroni), and reported as mean and standard deviation. During the toxicology study, variables with normal distributions were analyzed using the Dunnett-test, otherwise the Steel-test was applied. The Fisher-exact test was applied to frequency data. All tests were two-sided and in all cases $p < 0.05$ were accepted as the lowest level of significance. Group means were calculated for continuous data and medians were calculated for discrete data (scores). Test statistics were calculated on the basis of exact values for means and pooled variances.

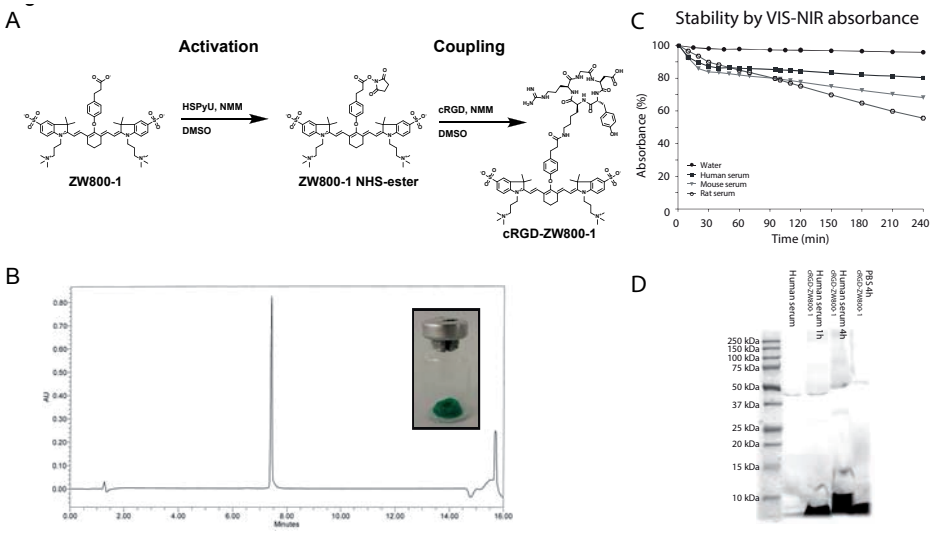

Figure 1 Structure, purity, stability and serum protein binding

A) Synthesis of cRGD-ZW800-1, which consisted of an activation step and a coupling step. B) Purity of the compound evaluated by UPLC-MS. Insert shows an example of the final lyophilized product. C) Stability of cRGD-ZW800-1 was measured in water and in human, mouse, and rat sera using VIS-NIR absorbance at 700nm. cRGD-ZW800-1 showed to be the most stable in water with a decrease in absorbance of only 4% at 4 h. D) cRGD-ZW800-1 was incubated in human serum for 1 and 4 h before gel electrophoresis was performed. At 4 h, one small additional band was seen around 45-50 kDa, which most likely represents the addition of cRGD-ZW800-1 molecules to serum proteins. The noticeable bands at 10-15 kDa are from contamination of the serum with heme, which is slightly fluorescent at 800 nm.

RESULTS

cGMP production of cRGD-ZW800-1

The NIR fluorophore ZW800-1 was prepared under cGMP conditions using previously described methods [23]. The procedure consists of 7 reaction steps and after each reaction the product was purified by precipitation. The linear RGD peptide was prepared by solid phase peptide synthesis. To comply with cGMP guidelines, the procedure for the cyclization and deprotection was adapted from procedures commonly used in literature (see supplementary data) [24]. Specifically, the normally used concentration steps (rotary evaporator) have been replaced by one precipitation after the deprotection. For the conjugation of ZW800-1 to cRGD, ZW800-1 was first activated as a reactive NHS ester (Figure 1A). Subsequently, the activated fluorophore was conjugated to cRGD, which was monitored using UPLC-MS (Figure 1B). After HPLC purification, cRGD-ZW800-1 was sterilely aliquoted in 10 mL glass vials and lyophilized, yielding 312 vials containing 0.725 mg of product.

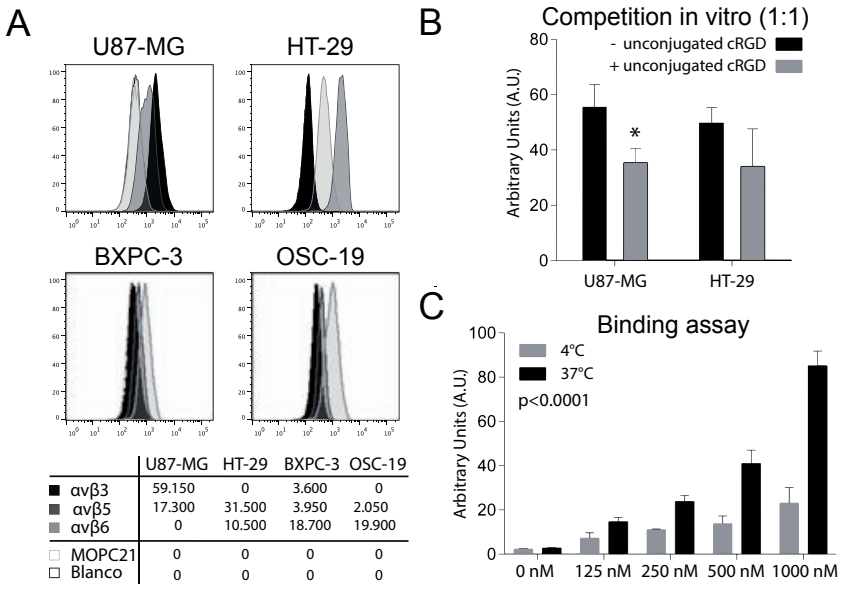

	U87-MG	HT-29	BXPC-3	OSC-19
αvβ3	59.150	0	3.600	0
αvβ5	17.300	31.500	3.950	2.050
αvβ6	0	10.500	18.700	19.900
MOPC21	0	0	0	0
Blanco	0	0	0	0

Figure 2 *In vitro* characterization of cell lines, competition, and binding assays
A) The number of antigenic sites for αvβ3, αvβ5, and αvβ6 integrins per individual cell of the U87-MG, HT-29-luc2, BXPC-3-luc2, and OSC-19-GFP-luc2 cell lines using Qifikit (DAKO) for quantitative flow cytometric analysis. B) *In vitro* competition experiment (1:1 ratio) using unlabeled cRGD (+ unconjugated cRGD) showing decreased NIR fluorescent signals in both the αvβ3 positive U87-MG (* p=0.05) as well as the αvβ3 negative HT-29-luc2 cell line (p=0.12) compared to the control without unlabeled cRGD (- unconjugated cRGD). C) Binding assay of cRGD-ZW800-1 on HT-29-luc2 cells showed enhanced signals when incubated at 37°C compared to 4°C with the various concentrations (p<0.0001). This may be the result of enhanced internalization of the agent.

Stability of cRGD-ZW800-1

The stability of cRGD-ZW800-1 was extensively evaluated in multiple ways: 1) in PBS using UPLC-MS (Figure S1); 2) in rat plasma using a Q-TRAP LC/MS/MS System (Figure S2); 3) in human serum using gel electrophoresis (Figure 1C); and 4) using VIS-NIR absorbance over time in water and in human, mouse, and rat sera (Figure 1D) and using full spectrum scan in water, water pH 7.4, and in Fetal Bovine Serum (Figure S3). Generally, no clinical relevant degradation was recognized (>95% intact after 4 h and >90% intact after 24 h), no degradation products were discovered and some addition to serum proteins was noticed.

The expression of αvβ3, αvβ5 and αvβ6 on tumor cell lines

As shown in Figure 2A, all 4 studied cell lines showed different expression levels. BxPC-3-luc2 expressed all 3 integrins, while HT-29-luc2, U87-MG, and OSC-19-GFP-luc2 expressed only 2 integrins. Overall, the U87-MG cells showed the highest, and OSC-19 cells the lowest, number of integrins.

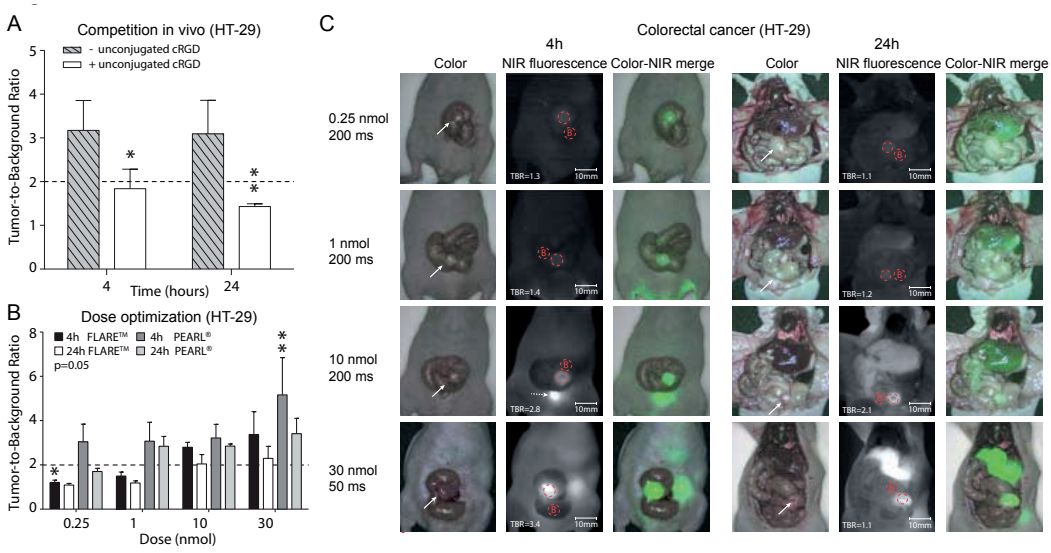

Figure 3 *In vivo* competition and dose optimization

A) *In vivo* competition experiment using a 200 times higher dose unlabeled cRGD compared to cRGD-ZW800-1 (1.24 mg, 2.0 µmol vs. 15.5 µg, 10 nmol) in the orthotopic HT-29-luc2 model. A significant decrease in TBR was seen between the group with co-injection of unlabeled cRGD and without both at 4 (* p=0.01) and 24 h (** p=0.004). B) Dose optimization showed reasonable TBRs (≥2) already with the 0.25 nmol (0.39 µg) dose group at 4 h with the Pearl® small animal imager. While using the clinically relevant FLARE® Prototype imaging system reasonable TBRs were seen from 10 nmol (15.5 µg) at both 4 h and 24 h. FLARE® Prototype and Pearl® differed significantly (p=0.05). Compared with the 10 nmol dose groups, significant differences were seen using the FLARE® Prototype at 4 h with 0.25 nmol (* p<0.01) and using the Pearl® at 4 h with 30 nmol (46.4 µg, ** p<0.01). C) Representative images captured with the FLARE® Prototype system of the various concentrations at 4 h and 24 h. For the 30 nmol dose group the exposure time had to be set at 50ms due to overexposure while for the other dose groups 200ms was sufficient. ROI tumor = red dotted circle, ROI background = red dotted circle with B, White arrow = tumor.

In vitro competition and binding assays

Competition for binding of cRGD-ZW800-1 (500 nM) with a 1:1 molar ratio of unlabeled cRGD (500 nM) resulted in a reduction of 40% in signal intensity on U87-MG cells (αvβ3, αvβ5 positive) and more than 30% on the HT-29-luc2 (αvβ5 and αvβ6 positive) cells while initial signal intensities were the same (Figure 2B). Furthermore, binding assays on HT-29-luc2 cells (Figure 2C) showed an almost linear increase in fluorescence intensity when increasing the concentration. Significant lower signals were observed when the cells were incubated at 4°C, preventing internalization of the agent.

In vivo binding characteristics on HT-29 (αvβ3 negative) tumor

An *in vivo* competition experiment was performed to validate binding specificity (Figure 3A). Significant higher TBRs were measured in the group without co-injection of

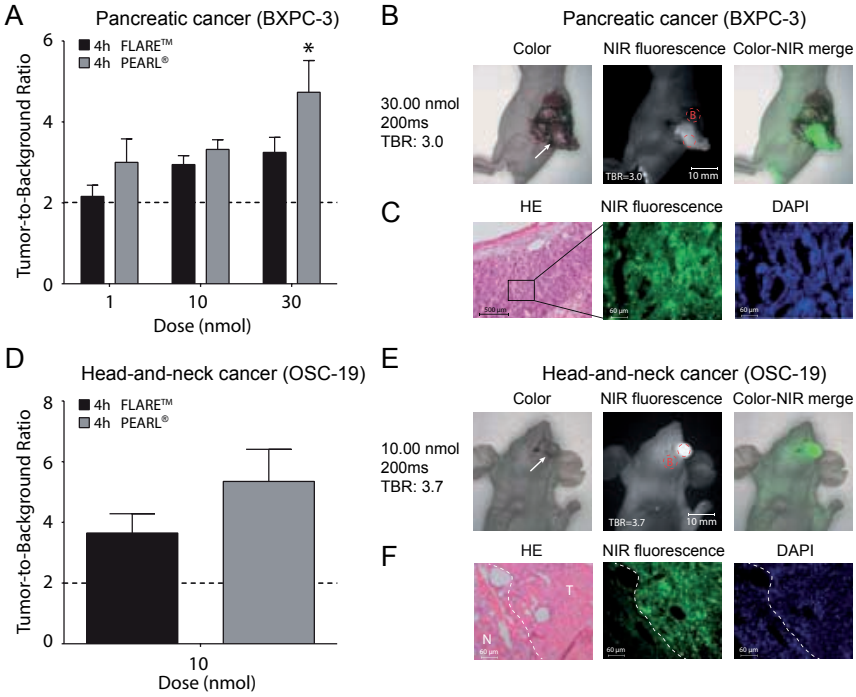

Figure 4 Clinical relevant orthotopic pancreatic and colorectal model

A) Mean tumor-to-background ratios at 4 h post injection in the BXPC-3-luc2 model calculated both with the Pearl® and the FLARE® Prototype system. Compared with the 10 nmol (15.5 µg) dose groups, only the 30 nmol (46.4 µg) dose group with the Pearl® was significantly higher (* $p<0.01$). B) Example showing the *in vivo* images of 30 nmol cRGD-ZW800-1 in the orthotopic pancreas model at 4 h post injection. ROI tumor = red dotted circle, ROI background = red dotted circle with B, white arrow = tumor C) NIR fluorescent microscopy of the validating the tumor specific NIR fluorescent signals of the *in vivo* model. D) Mean tumor-to-background ratios of the optimal dose 10 nmol at 4 h in the orthotopic head-and-neck cancer model. E) Example of images from the orthotopic OSC-19-GFP-luc2 model at 4 h. ROI tumor = red dotted circle, ROI background = red dotted circle with B, white arrow = tumor F) NIR fluorescent microscopy showing the border of a resected OSC-19-GFP-luc2 tumor. Clear fluorescent demarcation between normal and tumor tissue is shown (white dotted line). T = tumor & N = normal tissue surrounding the tumor

unlabeled cRGD (1.8±0.4 vs. 3.2±0.6, p=0.025) at 4 h, and increased at 24 h (1.4±0.1 vs. 3.1±0.6; p<0.001) The optimal dose was explored using both the Pearl® small animal imaging system and the FLARE® Prototype (Figure 3B). Overall, the Pearl® provided higher TBRs and the same trend was seen with increasing TBRs at higher doses and decreased TBRs after 24 h. Judging from the FLARE® Prototype, considering the required TBR of at least 2 and the high liver signals in the 30 nmol (46.4 µg) dose group, an optimal dose of 10 nmol (15.5 µg), with an imaging window of 4-24 h, could be set as starting point for future clinical translation (Figure 3C).

In vivo validation using BxPC-3-luc2 (αvβ3 positive) tumor

Tumor specific signals (TBRs >2) were observed at all 3 doses at 4 h post injection (Figure 4A). Figure 4B shows an example of a pancreatic tumor clearly delineated utilizing the FLARE® Prototype system. Fluorescence microscopy analysis revealed the co-expression of the NIR fluorescence signals with the malignant cells as shown in Figure 4C.

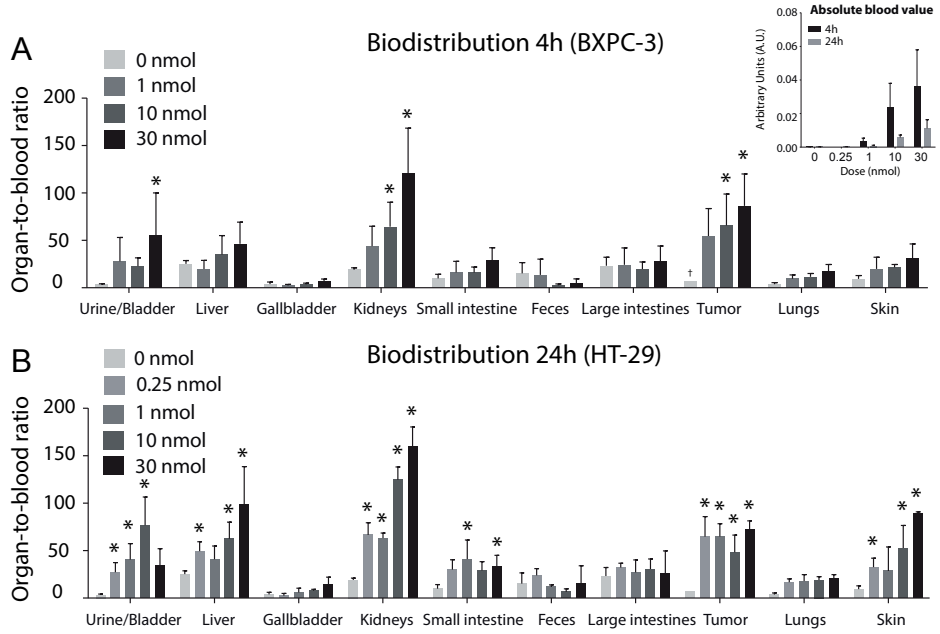

Figure 5 Biodistribution of cRGD-ZW800-1

A) Organ-to-blood ratios of cRGD-ZW800-1 at 4 h in the orthotopic pancreas model using 0, 1, 10, or 30 nmol (1.55, 15.5 and 46.4 µg respectively). Significance was seen between the control organs (0 nmol) and 30 nmol for bladder/urine (p<0.001), kidneys for 10 (p<0.001) and 30 nmol (p<0.001), and tumors for 10 (p<0.01) and 30 nmol (p<0.001) dose groups. Insert shows the absolute signals of blood at 4 h and 24 h. B) Organ-to-blood ratios of the used doses in the colorectal HT-29-luc2 orthotopic model. Asterisks indicates significant differences between control organ and various dose groups (p<0.05).

Orthotopic OSC-19-GFP-Luc2 head-and-neck cancer model (αvβ3 negative)

The optimal dose of 10 nmol (15.5 µg) cRGD-ZW800-1 was administered in the well-established tongue cancer model and resulted in clear tumor demarcation with a mean TBR of 5.4 ± 1.1 using the Pearl® and 3.7 ± 0.7 using the FLARE® Prototype (Figure 4D). Figure 4E shows an example of the model at 4 h post injection. Fluorescence microscopy of the tumor border showed clear demarcation with cRGD-ZW800-1 (Figure 4F).

In vivo biodistribution

At 4 h, higher doses showed similar or increasing ratios in the urine/bladder, liver, gallbladder, kidneys, large and small intestines, feces, tumor, lung, and skin (Figure 5A) while the other organs showed decreasing ratios (Figure S4A). Compared with the control animals, significant differences were seen for bladder/urine (30 nmol $p<0.001$), kidneys (10 nmol $p<0.001$ and 30 nmol $p<0.001$), and tumors (10 nmol $p<0.01$ and 30 nmol $p<0.001$). At 24 h, some autofluorescence was seen in the spleen and in the stomach, the latter mainly due to fluorescent food. Overall, in the HT-29-luc2 model, organ-to-blood ratios increased significantly ($p<0.05$) in urine/bladder, liver, kidneys, small intestine tumor, and skin with increasing doses (Figure 5B). NIR signals in the stomach, spleen, pancreas, heart, feces, large and small intestines, bone, muscle, cartilage, lungs, brain, and gallbladder remained similar or decreased (Figure S4B). Tumor-to-blood ratios are comparable between 4 and 24 h and showed mean values of 68.9±13.2 and 62.6±8.8 respectively. Relatively more fluorescence is present in the liver and the kidneys at 24 h compared to 4 h due to their metabolizing and eliminating functions. In addition,

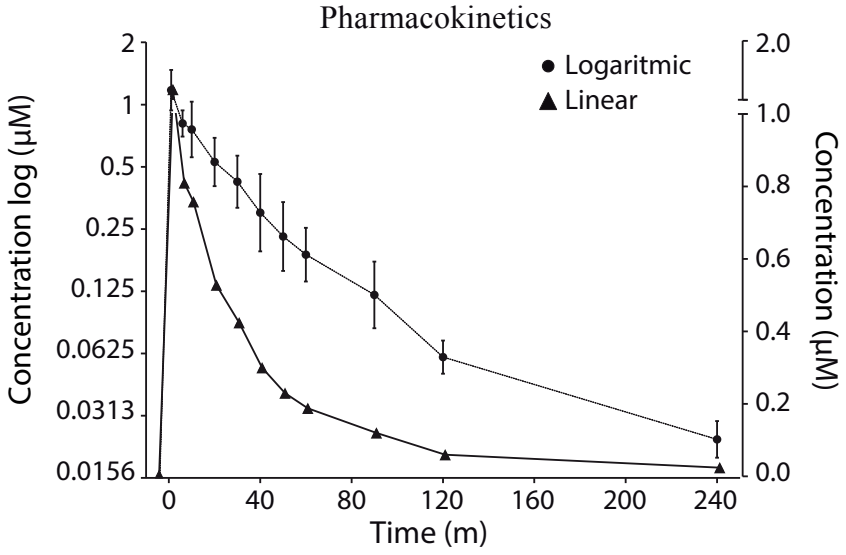

Figure 7 Pharmacokinetics of cRGD-ZW800-1

A) Graph shows the mean absolute concentrations (in µM) of cRGD-ZW800-1 either using a logarithmic axis (left y-axis) or a linear axis (right y-axis) up to 240 min post injection.

the skin also shows higher ratios at 24 h compared to 4 h, due to the binding of cRGD-ZW800-1 to integrins present in the skin. Examples of fluorescent images are shown in Figure S5.

Pharmacokinetics

The mean maximal concentration measured after 1 minute was 1.17 μM (Figure 6A and Figure S6 for individual values), measured fluorescent values were validated by a predefined calibration curve (Figure S7). The area under the curve (AUC), calculated via trapezoid rule, was 38.9±8.0. Clearance was 0.25±0.05 mL/min. After an initial distribution phase (half-life 14.6±1.5 min), pharmacokinetics of cRGD-ZW800-1 was linear (half-life 25.3±5.7 min) (Table S1).

Toxicity Studies

No treatment-related mortality occurred, and no effects compared to the control group on body weight (Figure S8), food consumption, hematology (Table S2), clinical biochemistry (Table S3) or macroscopic and microscopic alterations were observed. Discolored (green) urine was observed with 5.0 or 15.0 mg/kg doses on the day of treatment and in the first 3 days. One accidental death (control male at day 2) occurred due to blood sampling and no clinical signs, no findings on clinical pathology or microscopic findings indicating cause of death were noted. Microscopic findings at the injection site (tail vein) included perivascular inflammation, perivascular hemorrhage, and vascular necrosis and were present at similar incidence and severity in control and treated rats. These were considered procedure- rather than treatment-related. Based on these results, it is concluded that a single dose of 5.0 mg/kg and 15.0 mg/kg (with a NOAEL of at least 5.0 mg/kg) is well tolerated in rats.

DISCUSSION

In the search for accurate real-time tumor detection and diagnosis, NIR fluorescent imaging agents offer great potential. In this study, cRGD-ZW800-1 showed to be highly specific, renally cleared, non-toxic, and provided an imaging window between 4 and 24 h when using preclinical and clinical intraoperative imaging systems. cRGD binds to multiple cells from different origins and can therefore be applied for imaging of theoretically almost all solid cancer types.

Research on RGD often focuses on the αvβ3 integrin and neoangiogenic endothelial cells. However, 7 other integrins are also able to bind the RGD sequence with αvβ3, αvβ5, and αvβ6 also expressed on malignant cells [25-27]. This explains why cRGD-ZW800-1 accumulates in HT-29-luc2 and OSC-19-GFP-luc2 tumors: both are αvβ3 negative, but

exhibit high expression of integrins αvβ6 and αvβ8. The specific origin of these signals could be extracted from *in vitro* and *in vivo* blocking experiments, ruling out possible nonspecific accumulation, such as the enhanced permeability and retention effect [28]. Interestingly, no significant differences in TBRs between the three models were noticed. Although the biodistribution of cRGD-ZW800-1 showed some retention of fluorescence signals in the liver over time, possibly due to binding to serum proteins, no significant tracer accumulation in the intestines or gallbladder was observed during the investigated time frame. Similar results were found in clinical RGD based PET studies that showed higher intensity signals in the kidneys and urine, compatible with exclusive renal elimination [29]. Clearance patterns are important as limited target expression often constrains maximal tumor specific signals. Therefore, reduction of background signals is an important factor in improving TBRs [10]. The RGD binding motif is evolutionary conserved in humans, dogs, hamsters, mice, and rats [30]. Due to these similarities, the mouse xenograft and rat models provide valuable information about what can be expected during first-in-human studies. For example, fibroblasts in the skin express αvβ3 to interact with extracellular matrix proteins, resulting in uptake of cRGD-ZW800-1 in the skin as clearly seen during our biodistribution studies [31, 32].

cRGD-ZW800-1 is internalized into the cells after binding, as shown by fluorescence microscopy and *in vitro* binding assays, leading to the relatively large imaging window from 4-24 h post-injection. After internalization, the majority of integrins are recycled back to the cellular membrane in approximately 45 min [33]. Combined with the cRGD-ZW800-1 serum half-life value of approximately 25 min, we can rationalize that the majority of the compound is internalized during the first 45 minutes and therefore the absolute signal is dependent on the amount of primarily available agent and integrins rather than accumulation of the agent over time. The loss (20%) of NIR fluorescence signal in human serum in the first 4 h, most likely explained by the labile central oxygen linking modality of ZW800-1 [34], is therefore of minimal influence. Moreover, intracellular signals appear to be unaffected and remain up to 48 h [22, 34].

The toxicology experimental setup that is recognized by international guidelines as a recommended test system (e.g. OECD, FDA, EMEA, and MHW) was used. The tested dose of 5.0 mg/kg did not lead to any clinical symptoms, nor to cRGD-ZW800-1 related histopathological, biochemical, and hematological abnormalities. Thus, the no observable adverse event level (NOAEL) in rats is at least 5.0 mg/kg. Adjusting for body surface area (BSA) this results in a human equivalent dose of 0.80 mg/kg [35]. The FDA recommends to use 1/10 of the BSA-scaled lethal dose for 10% of test animals (LD10) to determine a safe starting dose [36]. Being very conservative, a dose of 80 µg/kg can therefore be considered as a safe starting dose for first in-human experiments. Further, adjusting the optimal dose in mice (10-30 nmol) into the human-equivalent dose shows the same starting dose range (63-188 µg/kg). No serious side effects were shown in clinical studies

with cilengitide (cRGDfK, MW: 589 Da), in which 2.0 g was intravenously administered twice weekly for a period up to 2 years [37]. Furthermore, ZW800-1 was extensively evaluated and showed no toxicity or adverse events in animal toxicity studies (unpublished data) using at least hundred times the intended doses.

A major challenge for the broad clinical introduction of fluorescence-guided surgery comprises the development of dedicated tumor-specific NIR fluorescent agents evaluated in combination with a clinical NIR camera system [38, 39]. Therefore, we evaluated all animals both with the preclinical Pearl® and the intraoperative FLARE® Prototype system. Generally, the Pearl® provided significant higher TBRs in all animal models for all doses, which is mainly a result of its optimized settings (e.g. long exposure times) and the use of a closed dark box [40]. Intraoperative real-time imaging is limited to exposure times of maximal 200 ms, which is 5 frames per second, to ensure smooth video images. After approval by local regulatory boards, cRGD-ZW800-1 will advance to clinical trials. The first phase will be a randomized, double-blind, placebo-controlled, single ascending dose study to assess safety, tolerability, and pharmacokinetics in healthy volunteers. The second phase will be an open label, single ascending dose, and exploratory study of cRGD-ZW800-1 in cancer patients.

This study describes the process needed to use the small peptide cRGD-ZW800-1 for clinical application. cRGD-ZW800-1 showed to possess a NOAEL of at least 5.0 mg/kg in rats which is comparable with a safe dose of 80 µg/kg in humans. In conclusion, cRGD-ZW800-1 forms a powerful imaging tool: with high affinity for either the cancer cells, the supporting endothelial cells, or both cell types. This property broadens the applicability of this probe since a large majority of tumors can be recognized.

REFERENCES

1. Vahrmeijer AL, Hutteman M, van der Vorst JR, van de Velde CJ, Frangioni JV. Image-guided cancer surgery using near-infrared fluorescence. Nat Rev Clin Oncol 2013;10: 507-18.
2. Sevick-Muraca EM, Houston JP, Gurfinkel M. Fluorescence-enhanced, near infrared diagnostic imaging with contrast agents. Curr Opin Chem Biol 2002;6:642-50.
3. Kelloff GJ, Krohn KA, Larson SM, et al. The progress and promise of molecular imaging probes in oncologic drug development. Clin Cancer Res 2005;11:7967-85.
4. Choi HS, Gibbs SL, Lee JH, et al. Targeted zwitterionic near-infrared fluorophores for improved optical imaging. Nat Biotechnol 2013;31:148-53.
5. Burggraaf J, Kamerling IMC, Gordon PB, et al. Detection of colorectal neoplasia *in vivo* in humans using an intravenously administered fluorescent peptide targeted against c-Met and fluorescence colonoscopy; a proof of concept study. Nat Med 2015.
6. van Dam GM, Themelis G, Crane LM, et al. Intraoperative tumor-specific fluorescence imaging in ovarian cancer by folate receptor-alpha targeting: first in-human results. Nat Med 2011;17:1315-9.
7. Vergote IB, Marth C, Coleman RL. Role of the folate receptor in ovarian cancer treatment: evidence, mechanism, and clinical implications. Cancer Metastasis Rev 2015.
8. O'Shannessy DJ, Somers EB, Albone E, et al. Characterization of the human folate receptor alpha via novel antibody-based probes. Oncotarget 2011;2:1227-43.
9. Chance B. Near-infrared images using continuous, phase-modulated, and pulsed light with quantitation of blood and blood oxygenation. Ann N Y Acad Sci 1998;838: 29-45.
10. Choi HS, Nasr K, Alyabyev S, et al. Synthesis and *in vivo* fate of zwitterionic near-infrared fluorophores1. Angew Chem Int Ed Engl 2011;50:6258-63.
11. Naumov GN, Akslen LA, Folkman J. Role of angiogenesis in human tumor dormancy: animal models of the angiogenic switch. Cell Cycle 2006;5:1779-87.
12. Schittenhelm J, Klein A, Tatagiba MS, et al. Comparing the expression of integrins alphavbeta3, alphavbeta5, alphavbeta6, alphavbeta8, fibronectin and fibrinogen in human brain metastases and their corresponding primary tumors. Int J Clin Exp Pathol 2013;6:2719-32.
13. Beer AJ, Haubner R, Sarbia M, et al. Positron emission tomography using [18F]Galacto-RGD identifies the level of integrin alpha(v) beta3 expression in man. Clin Cancer Res 2006;12:3942-9.
14. Beer AJ, Lorenzen S, Metz S, et al. Comparison of integrin alphaVbeta3 expression and glucose metabolism in primary and metastatic lesions in cancer patients: a PET study using 18F-galacto-RGD and 18F-FDG. J Nucl Med 2008;49:22-9.
15. Beer AJ, Niemeyer M, Carlsen J, et al. Patterns of alphavbeta3 expression in primary and metastatic human breast cancer as shown by 18F-Galacto-RGD PET. J Nucl Med 2008;49: 255-9.
16. Kenny LM, Coombes RC, Oulie I, et al. Phase I trial of the positron-emitting Arg-Gly-Asp (RGD) peptide radioligand 18F-AH111585 in breast cancer patients. J Nucl Med 2008;49: 879-86.
17. Bach-Gansmo T, Bogsrud TV, Skretting A. Integrin scintimammography using a dedicated breast imaging, solid-state gamma-camera and (99m)Tc-labelled NC100692. Clin Physiol Funct Imaging 2008; 28:235-9.
18. Axelsson R, Bach-Gansmo T, Castell-Conesa J, McParland BJ. An open-label, multicenter, phase 2a study to assess the feasibility of imaging metastases in late-stage cancer patients with the alpha v beta 3-selective angiogenesis imaging agent 99mTc-NC100692. Acta Radiol 2010;51:40-6.

19. Doss M, Kolb HC, Zhang JJ, et al. Biodistribution and radiation dosimetry of the integrin marker 18F-RGD-K5 determined from whole-body PET/CT in monkeys and humans. J Nucl Med 2012;53:787-95.
20. Manegold C, Vansteenkiste J, Cardenal F, et al. Randomized phase II study of three doses of the integrin inhibitor cilengitide versus docetaxel as second-line treatment for patients with advanced non-small-cell lung cancer. Invest New Drugs 2013;31:175-82.
21. Huang R, Vider J, Kovar JL, et al. Integrin alphavbeta3-targeted IRDye 800CW near-infrared imaging of glioblastoma. Clin Cancer Res 2012;18:5731-40.
22. Verbeek FP, van der Vorst JR, Tummers QR, et al. Near-Infrared Fluorescence Imaging of Both Colorectal Cancer and Ureters Using a Low-Dose Integrin Targeted Probe. Ann Surg Oncol 2014.
23. Hyun H, Bordo MW, Nasr K, et al. cGMP-Compatible preparative scale synthesis of near-infrared fluorophores. Contrast Media Mol Imaging 2012;7:516-24.
24. Bunschoten A, Buckle T, Visser NL, et al. Multimodal interventional molecular imaging of tumor margins and distant metastases by targeting alphavbeta3 integrin. Chembiochem 2012;13:1039-45.
25. Ruoslahti E. RGD and other recognition sequences for integrins. Annu Rev Cell Dev Biol 1996;12:697-715.
26. Humphries JD, Byron A, Humphries MJ. Integrin ligands at a glance. J Cell Sci 2006; 119:3901-3.
27. Brooks PC, Montgomery AM, Rosenfeld M, et al. Integrin alpha v beta 3 antagonists promote tumor regression by inducing apoptosis of angiogenic blood vessels. Cell 1994;79:1157-64.
28. Fang J, Nakamura H, Maeda H. The EPR effect: Unique features of tumor blood vessels for drug delivery, factors involved, and limitations and augmentation of the effect. Adv Drug Deliv Rev 2011;63:136-51.
29. Beer AJ, Haubner R, Goebel M, et al. Biodistribution and pharmacokinetics of the alphavbeta3-selective tracer 18F-galacto-RGD in cancer patients. J Nucl Med 2005;46: 1333-41.
30. Murakawa M, Okamura T, Kamura T, Shibuya T, Harada M, Niho Y. Diversity of primary structures of the carboxy-terminal regions of mammalian fibrinogen A alpha-chains. Characterization of the partial nucleotide and deduced amino acid sequences in five mammalian species; rhesus monkey, pig, dog, mouse and Syrian hamster. Thromb Haemost 1993;69:351-60.
31. Qin Z, Fisher GJ, Quan T. Cysteine-rich protein 61 (CCN1) domain-specific stimulation of matrix metalloproteinase-1 expression through alphaVbeta3 integrin in human skin fibroblasts. J Biol Chem 2013;288:12386-94.
32. Adams JC, Watt FM. Expression of beta 1, beta 3, beta 4, and beta 5 integrins by human epidermal keratinocytes and non-differentiating keratinocytes. J Cell Biol 1991;115:829-41.
33. Morgan MR, Hamidi H, Bass MD, Warwood S, Ballestrem C, Humphries MJ. Syndecan-4 phosphorylation is a control point for integrin recycling. Dev Cell 2013;24:472-85.
34. Hyun H, Owens EA, Narayana L, et al. Central C-C Bonding Increases Optical and Chemical Stability of NIR Fluorophores. RSC Adv 2014; 4:58762-8.
35. Reagan-Shaw S, Nihal M, Ahmad N. Dose translation from animal to human studies revisited. FASEB J 2008;22:659-61.
36. CDER. Guidance for industry. Estimating the maximum safe starting dose in initial clinical trials for therapeutics in adult healthy volunteers. 2005.
37. Stupp R, Hegi ME, Gorlia T, et al. Cilengitide combined with standard treatment for patients with newly diagnosed glioblastoma with methylated MGMT promoter (CENTRIC EORTC 26071-22072 study): a multicentre, randomised, open-label, phase 3 trial. Lancet Oncol 2014;15:1100-8.
38. Hwang J, Ramella-Roman JC, Nordstrom R. Introduction: feature issue on phantoms for the performance evaluation and validation of optical medical imaging devices. Biomed Opt Express 2012;3:1399-403.

39. Rosenthal EL, Warram JM, de BE, et al. Successful Translation of Fluorescence Navigation During Oncologic Surgery: A Consensus Report. J Nucl Med 2016;57: 144-50.
40. van Driel PB, van de Giessen M, Boonstra MC, et al. Characterization and Evaluation of the Artemis Camera for Fluorescence-Guided Cancer Surgery. Mol Imaging Biol 2014.
41. Boonstra MC, Tolner B, Schaafsma BE, et al. Preclinical evaluation of a novel CEA-targeting near-infrared fluorescent tracer delineating colorectal and pancreatic tumors. Int J Cancer 2015;137:1910-20.
42. van Driel PB, van der Vorst JR, Verbeek FP, et al. Intraoperative fluorescence delineation of head and neck cancer with a fluorescent anti-epidermal growth factor receptor nanobody. Int J Cancer 2014;134:2663-73.
43. Boonstra MC, van Driel PB, van Willigen DM, et al. uPAR-targeted multimodal tracer for pre- and intraoperative imaging in cancer surgery. Oncotarget 2015;6:14260-73.
44. Tseng W, Leong X, Engleman E. Orthotopic mouse model of colorectal cancer. J Vis Exp 2007;484.
45. Kim MP, Evans DB, Wang H, Abbruzzese JL, Fleming JB, Gallick GE. Generation of orthotopic and heterotopic human pancreatic cancer xenografts in immunodeficient mice. Nat Protoc 2009;4:1670-80.
46. Troyan SL, Kianzad V, Gibbs-Strauss SL, et al. The FLARE intraoperative near-infrared fluorescence imaging system: a first-in-human clinical trial in breast cancer sentinel lymph node mapping. Ann Surg Oncol 2009; 16:2943-52.